Thermo-electro-mechanical behavior of dielectric elastomer actuators: experimental investigations, modeling and simulation

Mario Kleo[1], Florentine Förster-Zügel[2] , Helmut F Schlaak[2] and Thomas Wallmersperger[1]

[1] Institut für Festkörpermechanik, Technische Universität Dresden, 01062 Dresden, Germany
[2] Microtechnology and Electromechanical Systems Laboratory, Technische Universität Darmstadt, 64283 Darmstadt, Germany

E-mail: thomas.wallmersperger@tu-dresden.de

CrossMark

Abstract

Dielectric Elastomer Actuators (DEAs) are elastic parallel plate capacitors consisting of polymers as dielectric layer and compliant electrodes'. In dynamic applications with high frequencies DEAs heat up. In this work the heating is studied by experimental investigations as well as by modeling of the visco-elastic behavior of the polymer and the specific electric resistance of the electrode and of the polymer. The experimental investigations have also been performed, in order to obtain parameters for the material model. A partially coupled thermo-electro-mechanical material model is presented and used for the numerical simulations. The experimental and numerical results for the time-dependent thermal behavior show an excellent qualitative correlation. This confirms the quality of the developed multi-field model.

(Some figures may appear in colour only in the online journal)

1. Introduction and state of the art

Dielectric elastomer actuators (DEAs) are smart structures, which are built as compliant capacitors with an elastic dielectric layer sandwiched between two compliant electrodes', made from graphite [1], metal [2] or carbon nanotubes [3, 4]. By applying an electric potential, the electrostatic attraction between the electrodes' leads to a deformation of the elastic dielectric structure. The working principle of DEAs is shown in figure 1.

The dielectric elastomer film contracts in thickness direction and, as it is incompressible, expands in lateral direction.

Detailed information on the capabilities and properties of DEAs are given in Carpi *et al* [5]. The operation principle is already well known. An early description of experiments with rubber as dielectric material can be found in the publication of Röntgen [6] from 1880. Due to progress in material sciences and fabrication methods, investigations of dielectric elasomers came back to interest, leading to an early modeling approach of Pelrine *et al* [7]. In 2000, Kornbluh *et al* [8] referred to viscoelastic behavior but still used Pelrine's linear elastic modeling approach. Some early experimental investigations, including viscoelastic behavior, were performed by Benslimane and Gravesen [9]. The need for considering the viscous contributions into the mechanical models for the simulation of DEAs were recognized and implemented for example in the model by Ask *et al* [10]. This model is based on the multiplicative split of the deformation gradient into elastic and viscous components and an additively splitted energy function,
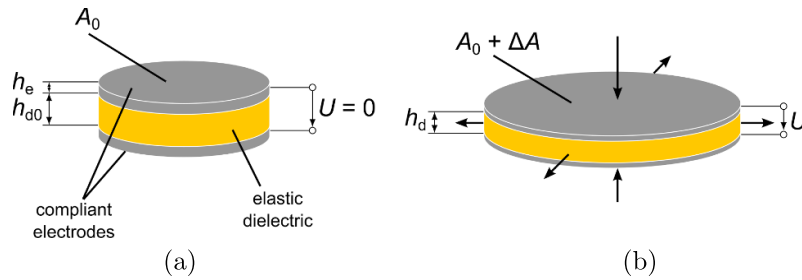
Figure 1. Structure and working principle of a dielectric elastomer actuator. (a) initial state, (b) deformed state after applying an electrical voltage to the electrodes'.

including contributions for elastic and viscous response. A non-linear numerical model for visco-electroelasticity was presented by Büschel *et al* [11] by regarding hyperelasticity. Mößinger *et al* [12] used an extended lumped parameter model including damping, for numerical investigations of the transient electromechanical behavior of DEAs. A model in analogy to the Kelvin-Voigt model, with additive decomposition of the Piola-Kirchhoff stress tensor, was shown by Madsen *et al* [13]. In a model of Schlögl and Leyendecker [14] the damping parameter dependent viscous amount is represented by an additive split of the Piola-Kirchhoff stress tensor. The model used in this paper equals the one used from Wissler and Mazza in [15]. Here, a Prony series is used to implement time dependent behavior. A different approach was used in the thermodynamic model from Lucking Bigué *et al* [16], by employing experimental loss factors, providing an amount of power 'lost' or rather transformed into heat.

Previous experimental investigations have shown, that excitations with fast alternating voltages, lead to a significant heating of a DEA [17]. Localized heating due to *spikes in* [electric] *current* where observed from Dudata *et al* [18]. Christensen *et al* [19] presented an electro-thermal model to analyze the thermal breakdown, depending on the number of layers in a stack actuator. In this model only resistive heating is studied. By also considering the mechanical deformation, a thermo-electro-mechanical model has been developed and presented in [20].

The aim of the present investigation is to study the primary causes for power loss and enhance the simulation model by experimental data, to explain the observed heating of a given DE-structure undergoing a cyclic load.

2. Experimental investigations

In order to be able to select an adequate material model for the numerical simulation of DEAs, its behavior has to be investigated experimentally. The behavior is based on the structure and the working principle of the DEA and can be divided into a mechanical and an electrical part. With the experimental investigations described in this section the mechanical and electrical material behavior of a sample DEA will be determined.

The structure of the sample DEA is shown in figure 2 and its geometrical parameters are listed in table 1. It consists of 49 stacked elastic dielectric layers with an active area of 40 mm
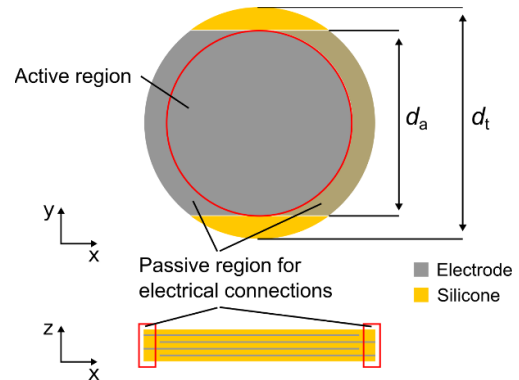

Figure 2. Top view and cross section of the sample multilayer DEA.

Table 1. Parameters of a DEA module.

Description	Value
Number of active dielectric layers n	49
Thickness of dielectric layer h_{d0}	45 μm
Thickness of graphite electrode h_e	5 μm
Diameter of active area d_a	40 mm
Total diameter d_t	50 mm

diameter. For the electrical connections of the 50 electrodes', the active area is surrounded by a 5 mm passive region. The thickness of the elastic dielectric layers h_d is 45 μm, the thickness of the electrode layers h_e is 5 μm. Hence, the thickness of the whole DEA is about 2.5 mm. The dielectric layers are made of the silicone ELASTOSIL® P7670 from Wacker Chemie AG. The electrodes' consist of graphite particles MF2 from NGS Naturgraphit GmbH. For connecting the electrode layers, copper wires are put into the passive electrode area.

2.1. Mechanical behavior of dielectric elastomers

The mechanical behavior of the DEA primarily results from the mechanical properties of the elastomer. The silicone used as elastic dielectric shows an elastic and viscoelastic behavior. It behaves isotropic and is incompressible with a Poisson's ratio of $\nu \approx 0.5$.

The deformation behavior of an elastomer can be represented by a stress-strain curve. To obtain this curve, a uniaxial compression test with the measurement setup shown in figure 3 is carried out. The compression tests were performed
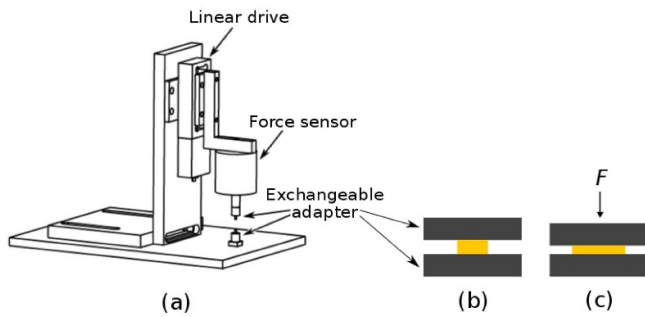
Figure 3. (a) Measurement setup for uniaxial compression tests, (b) adapter and test sample before testing and (c) during testing.
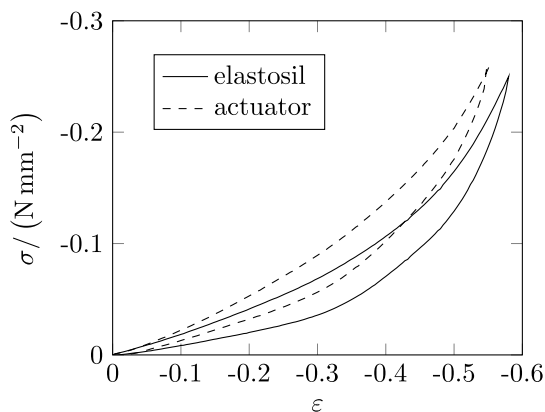

Figure 4. Stress-strain diagram of the uniaxial compression test, the duration of one cycle is 290 s.

to reach deformations which resemble the ones during operation. For testing, samples of ELASTOSIL® P7670 with 2.5 mm thickness and 5.8 mm diameter are prepared. The test samples are compressed between the lubricated adapters with a velocity of 0.01 mm s^{-1} and the resulting force is measured. The engineering stress is calculated by dividing the measured force by the size of the initial area on which the force is acting. The engineering strain is calculated by dividing the length change by the initial length of the sample.

Although the mechanical behavior of the DEA primarily results from the mechanical properties of the elastomer, the influence of the graphite powder electrodes' should be known. Because it is not possible to do the compression tests with loose graphite powder, test samples with the same dimensions as the silicone test samples are cut out of the active area of a DEA and again the uniaxial compression test is carried out. Figure 4 shows the obtained stress-strains curves of the pure ELASTOSIL® P7670 and the actuator test samples.

It can be seen that the graphite electrodes' in the DEA sample lead to a steeper stress-strain curve compared to the pure silicone sample. In addition, both curves show a hysteresis which is due to the viscoelastic properties of the silicone.

The time-dependent viscoelastic behavior is described by creep and relaxation processes. Creep means that if the elastomer is subjected to a constant mechanical stress step it responds with an initial strain step followed by an exponential increase of the strain over time. Relaxation is the asymptotic

decrease in stress over time after an initial stress step due to an applied strain step (see Zhao *et al* [21]).

For determining the viscoelastic behavior of the ELASTOSIL® P7670 and the DEA a creep test and a relaxation test were performed. For the creep test, a test sample was subjected to a constant force which results in an initial compression strain of about 20 %. During the relaxation test a constant compression strain of 25 % was applied to the test sample. Displacement respectively force were measured for 20 minutes. The determined creep and relaxation curves are shown in figures 5 and 6. The forces needed for a compression of about 20 % differ for the pure silicone sample and the actuator sample. In case of the actuator, the force needed is higher because as seen in the stress-strain curves the actuator behaves stiffer than the pure silicone due to the electrodes'. For this reason, the resulting stress in the actuator is higher for a constant compression of 25 % as in the silicone sample. However, the silicone and the actuator samples show similar time-dependent creep and relaxation behavior.

2.2. Electrical behavior of dielectric elastomers

The DEA setup can be transformed into an electrical equivalent circuit, which is shown in figure 7. It consists of the capacitance C_a, the parallel resistance of the dielectric polymers layers R_p which causes the leakage current and the series resistance R_s which includes the electrode resistances and the contact resistances of the electrical connections [22].

The value of the capacitance C_a can be calculated by

$$C_a = \epsilon_0 \epsilon_r \frac{A}{h_d}. \tag{1}$$

It is defined by the material properties of the elastic dielectric (vacuum permittivity ε_0, relative permittivity ϵ_r) and the actuator design (active region A, thickness of the dielectric layer h_d).

A direct measurement of the relative permittivity ϵ_r of the dielectric layer is impossible. Therefore, a sample structure is fabricated. Copper electrodes' with a defined size are sputtered on a silicone membrane with 50 μm thickness. With an LCR meter the capacitance of the sample structure is measured and the relative permittivity is calculated after rearranging equation (1):

$$\epsilon_r = \frac{1}{\epsilon_0} \frac{C h_d}{A} \tag{2}$$

The value of the calculated relative permittivity ϵ_r of ELASTOSIL® P7670 is 3.

In general, the value of the parallel resistance R_p of unmodified silicone material is of the order of gigaohms up to teraohms. For ELASTOSIL® P7670 R_p is about 40 GΩ [23]. With $\rho_d = R_p A / h_d$ the specific resistance results to around 1 TΩ cm.

As already mentioned, the electrodes' consist of graphite powder particles. For this type of electrode a constant specific resistance, as it is valid for homogeneous materials, does
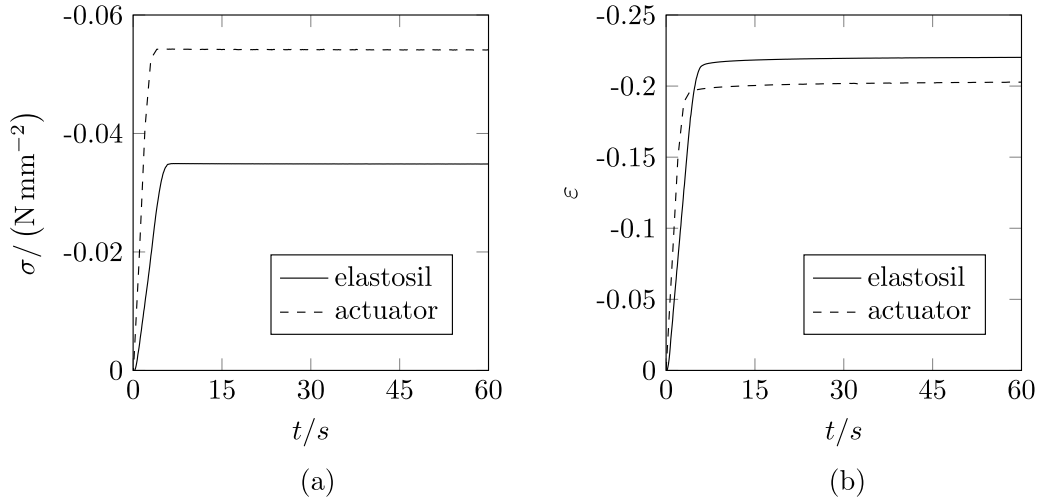
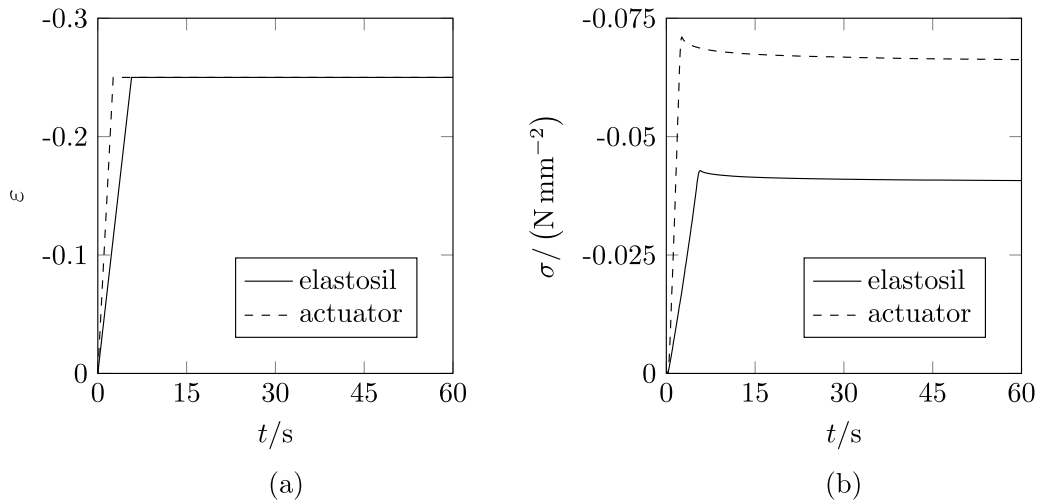**Figure 5.** Compression creep test of ELASTOSIL® P7670 and actuator, (a) stress vs. time, (b) strain vs. time.

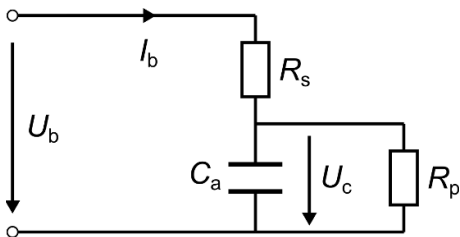**Figure 6.** Compression relaxation test of ELASTOSIL® P7670 and actuator, (a) strain vs. time, (b) stress vs. time.

Figure 7. DEA equivalent circuit with parallel resistance of the polymer..

not exist. But it is possible to measure the sheet resistance R_e which is defined as

$$R_e = \frac{\rho_e}{h_e} \qquad (3)$$

with ρ_e as specific resistance and h_e as electrode thickness. For the sheet resistance measurement a sheet resistance meter is used. The measured value for the graphite powder electrodes'

is 10 kΩ. By rearranging equation (3), the value of ρ_e is calculated. With the given electrode thickness of 5 μm the specific electrode resistance ρ_e results to 5 Ω cm.

In this work the contact resistances are neglected. But previous measurements have shown that the used type of electrical connection results in contact resistances at the transition from compliant electrodes' to the stiff copper wires between 10 kΩ and 80 kΩ [24].

2.3. Electro-Mechanical coupling

The application of an electric voltage to the DEA leads to an electrostatic attraction between the electrodes'. The effective electrostatic pressure $\tilde{p}_{el}$ can be calculated by [7]:

$$\tilde{p}_{el} = \epsilon_0 \epsilon_r \frac{U^2}{h_d^2} = \epsilon_0 \epsilon_r E^2 \qquad (4)$$

The electrostatic pressure depends on the relative permittivity ϵ_r of the elastomer, the applied voltage U and the thickness h_d of the dielectric elastomer layers. The voltage applied to the
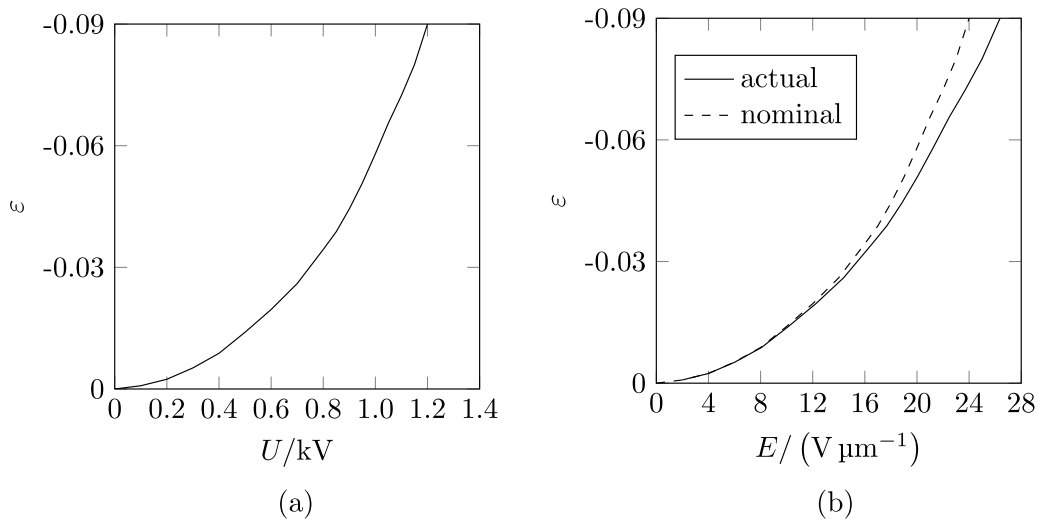
Figure 8. Characteristic deformation curve of actuator, (a) voltage versus strain and (b) electric field versus strain, here nominal means the electric field is calculated with $E_0 = U/h_{d0}$.
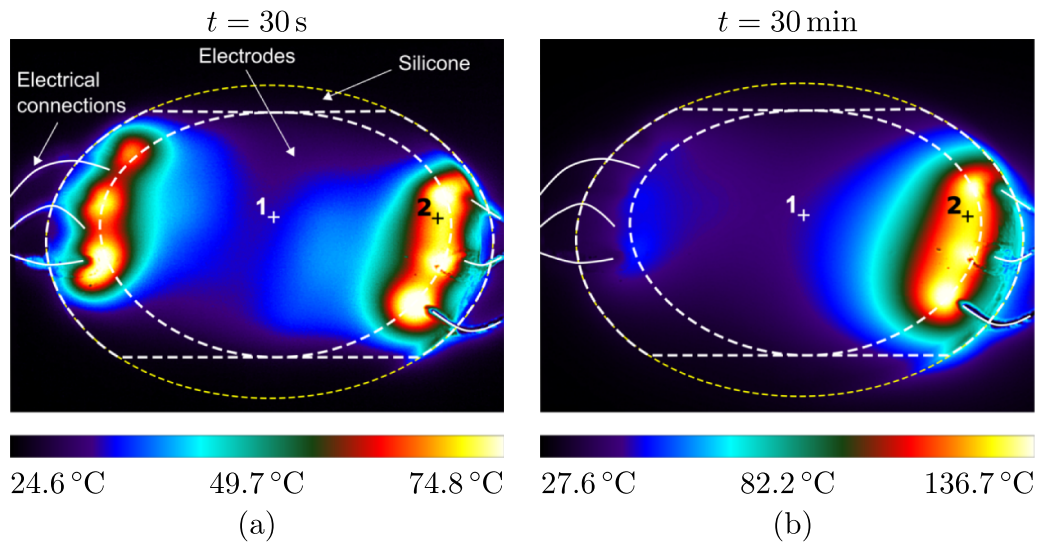

Figure 9. Thermal images of the sample DEA subjected to a dynamic excitation of 1 kV and 1 kHz, (a) after 30 seconds and (b) after 30 minutes. The sample actuator was filmed from the side.

DEA is restricted by the dielectric breakdown field strength of the elastomer. Taking into account the thickness h_d of the elastic layers and the breakdown field strength of the material a maximum voltage can be calculated. However, it is important to take into account the varying thickness of the layers.

After the application of the electric voltage the DEA deforms until the electrostatic pressure is balanced by the elastic pressure of the elastomer. The resulting deformation of the DEA depends on the mechanical material properties of the elastomer. The stiffer the material, the smaller the deformation.

Figure 8 shows the measured actuator strain depending on the applied electric voltage and field strength for the sample DEA introduced before. In figure 8(b), the straight line represents the electric field, i.e. the voltage over the actual thickness, and the dashed line the voltage over the initial thickness. This means that for a given strain the actual electric field

is larger than the prescribed nominal one. Due to the breakdown strength E_{EBS} of ELASTOSIL® P7670 with at least 30 V μm^{-1} the maximum applied voltage U during testing is 1200 V. This leads to an electric field strength E of around 26 V μm^{-1} taking into account the thickness change of the elastomer layers. At the maximum applied voltage the deformation of the DEA is about 9 %. For the thickness measurement two laser displacement sensors (Keyence LK-G32) are used. During actuation, the deformation of the DEA is measured from both sides [25].

2.4. Thermo-Electro-Mechanical coupling

Dielectric elastomer actuators heat up during operation. This heating up due to dynamic excitation is a thermo-electro-mechanical process. On the one hand this is due to the non-ideal conductivity of the electrodes' and the contact resistances
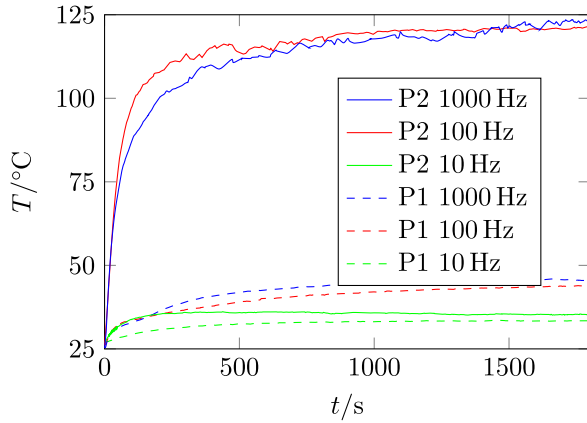
Figure 10. Heating of the test DEA due to the frequency of the applied voltage, at point No. 1 and Point No. 2. see figure 9, experimental data.

and on the other hand this is due to the visco-elasticity of the elastomer. During operation of the DEA, charging and discharging current is flowing through the electrodes' and a leakage current is flowing through the polymer. Because of the resistances, the electric current leads to a heating along the electrodes' and at the electrical connection of the DEA. In addition, heating in the elastomer material occurs due to the deformation of the material and the appearing internal friction of the molecules and due to joule heating. The increase of temperature in the DEA depends strongly on the dynamic excitation. In general, DEAs are used at frequencies f of the electric voltage from DC to around 1 kHz.

For measuring the heating of the sample actuator, a voltage U of 1 kV at frequencies f of 10 Hz, 100 Hz and 1 kHz is applied for 30 minutes to the electrodes'. During this time the temperature of the whole DEA is measured with a thermal imaging camera (FLIR SC655). Figure 9 shows the thermal images of the tested DEA after 30 seconds and 30 minutes operation with 1 kHz and 1 kV. A symmetric temperature distribution was obtained after 30 seconds, as expected. The temperature distribution after 30 minutes was not symmetric. This behavior may be caused by an uneven degradation of the left and the right electrical connections of the DEA. The temperatures at the two points marked in figure 9 are analyzed and the results are shown in figure 10. The diagrams show the influence of the frequency to the heating of the DEA. With increasing frequency the temperature in the actuator increases as well. In addition it can be seen, that during operation the DEA heats up slowly in the middle of the active area and much faster next to the electrical connections. For higher frequencies the area next to the connections reaches a temperature of almost 125 °C and the heating process seems not to be finished. The region in the middle of the actuator reaches temperatures between 33 °C and 45 °C.

3. Multi-Field model

In the present section, the physical models of the involved mechanical, electrical and thermal domains are presented.

Both, the coupling of the mechanical and electrical domain, as well as the mechanism of the resulting heating of the cyclic actuated structure are given.

3.1. Mechanical field

To evaluate the mechanical behavior of the DE structure, a model is needed, which is capable of describing visco-hyperelastic behavior. The aim of this section is, to (i) present the mechanical field equations and (ii) introduce the applied mechanical material model.

In the following equations the index notation is used, as well as the EINSTEIN summation convention for the coordinate indices $k, l, m = 1, 2, 3$. The deformation gradient tensor **F** is given by:

$$F_{kl} = \frac{\partial x_k(X_m, t)}{\partial X_l}. \tag{5}$$

Here, $\vec{x}$ represents the current position vector and $\vec{X}$ the referential position vector. The deformation gradient can be decomposed polarly into a rotational and a stretch component

$$F_{kl} = R_{km}U_{ml} = V_{km}R_{ml}, \tag{6}$$

where **R** is the rotation tensor, **U** is the (material) right stretch tensor and **V** is the (spatial) left stretch tensor. The eigenvalues of **U** and **V** are called the principal stretches λ_p. In this work, the material is assumed to be incompressible, which leads to

$$\lambda_1 \lambda_2 \lambda_3 = 1. \tag{7}$$

With the mass density ϱ, the CAUCHY stress tensor $\boldsymbol{\sigma}$ and the volume force density vector $\vec{f}$ the balance of momentum reads

$$\sigma_{lk,l} + \varrho f_k = \varrho \ddot{x}_k. \tag{8}$$

$\ddot{\vec{x}}$ is the second order time derivative of the current position vector. The symmetry of the stress tensor

$$\sigma_{kl} = \sigma_{lk}, \tag{9}$$

follows from the balance of angular momentum. Regarding the assumption of incompressibility, the hyperelastic material behavior can be described according to OGDEN [26], for which the strain energy density W is defined as

$$W(\lambda_1, \lambda_2, \lambda_3) = \sum_{i=1}^{N} \frac{\mu_i}{\alpha_i} \left[\lambda_1^{\alpha_i} + \lambda_2^{\alpha_i} + \lambda_3^{\alpha_i} - 3 \right], \tag{10}$$

with the material constants μ_i and α_i. By including time-dependence of the material parameters, represented in terms of PRONY series, a viscoelastic material behavior can be modeled [27].

$$\mu_i(t) = \mu_{i,\infty} \left[\beta_\infty + \sum_{j=1}^{M} \beta_j \exp\left(-\frac{t}{\tau_j}\right) \right] \tag{11}$$
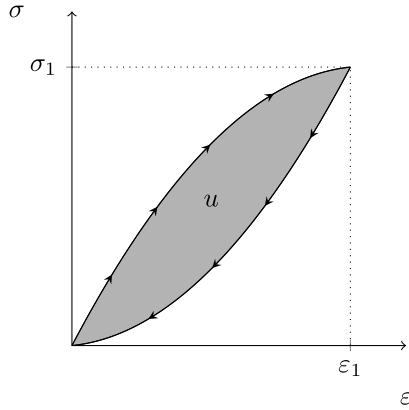
Figure 11. Schematic representation of the mechanical hysteresis of the viscoelastic behavior; the 'lost' energy density per cycle u is shown within the hysteresis loop.

The parameters for the PRONY series are β_∞, β_j and τ_j. The exponential decay in stiffness has been proved appropriate to model the mechanical behavior of silicone subjected to cyclic loads [28]. Thus, the principal values of the CAUCHY stress σ_p can be calculated as

$$\sigma_p = \lambda_{(p)} \frac{\partial W}{\partial \lambda_{(p)}} - \tilde{p}, \tag{12}$$

where $\tilde{p}$ is an arbitrary hydrostatic pressure introduced due to the incompressibility constraint equation (7). Please note, that there is no summation over indices given in brackets.

3.1.1. Dissipation in the mechanical field. To investigate the energy which is converted into the thermal energy during the actuation, the mechanical energy 'loss' has to be considered [29]. Therefore, we define the mechanical power density p^{mech} as

$$p^{\text{mech}} = \sigma \dot{\varepsilon}. \tag{13}$$

For further investigation we additively decompose the mechanical power into an elastic p^{ela} and a viscous part p^{vis}

$$p^{\text{mech}} = p^{\text{ela}} + p^{\text{vis}}. \tag{14}$$

In the case of cyclic loading, the sum of the elastic mechanical power vanishes over each cycle due to the equilibrium of the mechanical energy of the loading and unloading phase. The mean value of the viscous mechanical power density $\overline{p}^{\text{vis}}$ can be calculated from the potential energy density u lost in each cycle and the frequency of the mechanical loading function f^{mech}

$$\overline{p}^{\text{vis}} = u f^{\text{mech}}. \tag{15}$$

As shown in figure 11, the 'lost' potential mechanical energy density in each cycle, which is transferred into thermal energy, is equal to the area of the hysteresis in the stress-strain-diagram.

3.2. Electrical field

The electrical field formulation has to be considered in the two components of a DEA, (i) the polymer, where the electric potential leads to a polarization of the dielectric material and (ii) the electrode, where the electric charge is mobile. The balance laws of the electrical field are derived from MAXWELL's equations. If we neglect magnetic effects, the Maxwell-Faraday equation is defined as

$$e_{mlk} E_{l,m} = 0 \tag{16}$$

for which **e** represents the third order LEVI-CIVITA-tensor and $\vec{E}$ is the electric field vector. GAUSS's law

$$D_{k,k} = q^{\text{f}} \tag{17}$$

provides a relation between the electric displacement field $\vec{D}$ and the density of the free electrical charge q^{f}. From AMPÈRE's circuital law

$$j_k^{\text{f}} = -\dot{D}_k \tag{18}$$

we obtain the third balance equation, where $\vec{j^{\text{f}}}$ denotes the free current density. The continuity of charge provides the formal relation of charge and current

$$j_{k,k} = \left(j_k^{\text{f}} + j_k^{\text{b}}\right)_{,k} = -\frac{\partial q}{\partial t} = -\frac{\partial}{\partial t} \left(q^{\text{f}} + q^{\text{b}}\right). \tag{19}$$

Here, the superscript $(\cdot)^{\text{f}}$ and $(\cdot)^{\text{b}}$ stand for the free and bound parts of charge and its current. For the electric field in the dielectric material we assume a linear, isotropic material behavior

$$D_k = \epsilon_0 \epsilon_{\text{r}} E_k. \tag{20}$$

Here, ε_0 stands for the free space permittivity and ϵ_{r} for the relative permittivity. While charging and discharging, the constitutive equation for the current is given by

$$j_k^{\text{f}} = \frac{1}{\rho} E_k, \tag{21}$$

where ρ represents the respective specific resistance.

3.2.1. Dissipation in the electrical field. For the dissipation in the electrical field two effects have to be considered, the dielectric loss and the resistive loss.

The dielectric loss occurs, due to the fact of dielectric relaxation. The loss tangent (or the dissipation factor) is considered to be small for silicone rubbers within the investigated frequency range (with the maximum of 1 kHz) [30]. Thus the dielectric power loss is assumed to have a minor influence on the heating of the structure and will be neglected in this work.

The specific resistance of the electrode leads to a loss while charging and discharging the electrode layers. Due to the scales of frequency and the strength of the electric field invest-igated, for this work only the resistive loss is considered. The

power density of an electric current within an electric field p^{elec} is given by

$$p^{\text{elec}} = j_k^{\text{f}} E_k. \tag{22}$$

Considering the constitutive equation (21) the density of the resistive power loss p^{res} can be calculated by

$$p^{\text{res}} = \rho_e j_k^{\text{f}} j_k^{\text{f}}, \tag{23}$$

if the current on the electrodes' is known. For the dissipation, resulting from the leakage current flowing through the polymer [31], we can determine the power loss density depending on the electric field in the dielectric material by

$$p^{\text{leak}} = \frac{1}{\rho_d} E_k E_k. \tag{24}$$

Figure 12. Illustration of the solution procedure.

3.3. Electro-Mechanical coupling

For the electro-mechanical coupling, we use the additive decomposition of the total stress tensor $\boldsymbol{\sigma}^{\text{tot}}$ into a mechanical part and the MAXWELL stress tensor [32]

$$\boldsymbol{\sigma}^{\text{tot}} = \boldsymbol{\sigma}^{\text{maxw}} + \boldsymbol{\sigma}^{\text{mech}}. \tag{25}$$

The mechanical stress tensor $\boldsymbol{\sigma}^{\text{mech}}$ is equal to the previously defined CAUCHY stress. The MAXWELL stress tensor $\boldsymbol{\sigma}^{\text{maxw}}$ is defined as

$$\sigma_{kl}^{\text{maxw}} = \epsilon E_k E_l - \frac{1}{2} \delta_{kl} \epsilon E_m E_m, \tag{26}$$

where $\epsilon = \epsilon_0 \epsilon_r$. Considering compliant electrodes, this formulation is consistent with the previously equivalent electrostatic pressure in equation (4).

3.4. Thermal field

Since DEAs are subjected to a heating and therefore a temperature change, the thermal field has to be incorporated. The thermal field is described by the heat equation

$$\varrho \chi \frac{\partial T}{\partial t} + \left(-\kappa T_{,k} + q_k^{\text{c}} \right)_{,k} = q^{\text{tot}}. \tag{27}$$

Here χ denotes the specific heat capacity, κ the thermal conductivity, T the temperature, $\vec{q}^{\text{c}}$ the convective heat flux vector and q^{tot} the total volumetric heat source. At the top and lateral surfaces of the DEA a convective cooling is assumed as boundary condition, which is dependent on the difference between surface (T^{s}) and ambient (T^{a}) temperature and the heat transfer coefficient α.

$$q_k^{\text{c}} = \alpha \left(T^{\text{s}} - T^{\text{a}} \right) n_k. \tag{28}$$

The heat transfer coefficient itself depends on the difference between surface and ambient temperature as well [33].

$$\alpha = \beta_T \left(T^{\text{s}} - T^{\text{a}} \right)^{0.25} \qquad \text{for top surface} \tag{29}$$

$$\alpha = \alpha_L + \beta_L \left(T^{\text{s}} - T^{\text{a}} \right)^{0.25} \qquad \text{for lateral surface} \tag{30}$$

Please note the different dimensions of α and β. The used values for the variables are given in table 3. The surface normal vector $\vec{n}$ is defined by the boundary of the thermal field. The former defined power losses in equations (15), (23) and (24) are supposed to completely transfer into heat

$$q^{\text{tot}} = p^{\text{vis}} + p^{\text{leak}} + p^{\text{res}}. \tag{31}$$

With these assumptions the thermal field is fully defined.

4. Numerical simulation

In this section, it is described, how the system of equations (presented in section 3) is solved numerically. Therefore, the numerical tools Matlab and ANSYS are used. Due to the different time scales of the processes regarding the respective fields, the computation was performed in several substeps. The thermal field, for example, is evaluated within a duration of 30 min, employing time steps of seconds. Much smaller time steps are necessary to compute the mechanical behavior with a cyclic excitation of up to 1000 Hz. A fully coupled analysis would have made it necessary to perform the simulation with time increments defined by the fastest process, leading to a vast amount of required computational power, to simulate the examined actuator.

For the numerical simulation in ANSYS two test cases are investigated, for which the geometrical parameters are given in table 2.

The first one (test case 1) uses a round electrode similar to that used by the DEA in the creep and relaxation test, described in section 2.1. Test case 2 is defined as the sample DEA, shown in figure 2, with alternating mirror symmetrical electrode design. Figure 12 shows the workflow of the numerical simulation, performed in this work, in order to calculate the heating of the actuator, resulting from the electromechanical excitations. First, the material model parameters are obtained from a curve fitting procedure, on the basis of

the experimental data given in section 2. Second, the mechanical material model is evaluated by numerical simulations using the finite elements software ANSYS. For that, the geometry of test case 1 is employed. As third step, a coupled transient electro-mechanical simulation is performed for the same test case. For this operation, the input is given by an application of a sinusoidal voltage on the electrodes'. As result we obtain the displacements as well as the stress σ and strain ε response versus time. From that data, the power loss due to the viscous loss p^{vis} is calculated. The data of the resulting electric field within the polymer is used to determine the power loss due to leakage current p^{leak}. Additionally, via the data of the electrodes' charge density q^{f}, the free current density $\vec{j}^{\mathrm{f}}$ at the electrode and derived from that the electrodes' resistive loss density p^{res} are computed, within the forth step of the solution procedure. Therefore, test case 2 is used for the simulation of the electrical charging and discharging of the electrode. For a thermal analysis (step five), in which (i) a constant input of thermal energy and (ii) a temperature-dependent convection is prescribed. The temperature in the probe increases with time resulting in a steady-state solution. The heat input is given with the power losses $p^{\mathrm{res}}, p^{\mathrm{leak}}$ and p^{vis} calculated in the previous steps. Convective cooling is applied on the upper and lateral surface. This simulation will provide the resulting temperature distribution versus time. To not unnecessarily inflate the calculations, the following assumptions are made:

4.1 Homogeneity of mechanical field

It is sufficient to only distinguish between the active and the passive domain, since the mechanical field is assumed to be homogeneous within the excited layers. The intersection of these domains with an inhomogeneous mechanical behavior is small in comparison to the rest, so that by neglecting this *intermediate domain* the occurring inaccuracy will be insignificant.

4.2 Neglecting of edge effects of electric field

The inhomogeneity of the electric field at the edges of the electrodes' will be neglected as well. The effective error is vanishingly small due to the ratio of electrodes' area to the distance between electrodes' [34, 35].

5. Parameter identification, results and validation

The experimental investigations performed in section 2 were used to obtain the necessary parameters for the material models in section 3, employed for the simulation described in section 4. In the present section, the simulation results are given. In section 5.1 the material parameters are provided. The correlation of experimental and numerical results of the mechanical behavior is given in section 5.2. In section 5.3, the results of the thermal simulations are given and validated with the experimentally gained heating curves for the investigated frequencies.

5.1. Parameter identification

The parameters for the mechanical model are obtained from a curve fitting procedure between the mechanical material model and the experimental data of the relaxation test. The mass density of ELASTOSIL® P7670 is taken from the manufacturer data sheet [36]. The mass density of the electrode is assumed to be equal to the one of the polymer. Since we use the experimental data of the actuator, the mechanical model assumes a homogenized structure of the actuator in thickness direction. The electrical material properties were measured as described in section 2.2. The parameters for density, thermal conductivity and specific heat of silicone rubber were taken from results available in literature [37, 38]. Since the structure of the electrode is not exactly known, there exist no really reliable data. Empirical values have been used, resulting from previous numerical investigations. A list of the used material parameters is shown in table 3.

5.2. Results of the simulation of the electro-mechanical field

The results of the electro-mechanical simulation are presented in this section. The electrostatic attraction of the electrodes', due to the excitation with a sinusoidal voltage, leads to cyclic stress in thickness direction. The resulting strain becomes stationary after a certain number of cycles, as consequence of the viscous material behavior. The envelopes of the strain are displayed in figure 13, for the frequencies of $f = \{10\ \mathrm{Hz}, 100\ \mathrm{Hz}$ and $1000\ \mathrm{Hz}\}$. Since the difference of energy loss per cycle within the transient part is small with respect to the duration of the complete process, we only consider the stationary behavior for the subsequent analysis.

Figure 14 shows a hysteresis plot, resulting from the numerical simulation. Here, the difference of the loading and unloading phase in one cycle at the frequency of 1 kHz is given, for when this difference becomes stationary. The abscissa is given by the curve of the loading phase. The area within the curve is equal to the viscous energy lost per cycle, as described in section 3.1. Whereas the viscous power loss and the power loss due to leakage current are evenly distributed in the active domain, the electrodes' resistive power loss is not. The charging and discharging related current density on the electrode layer is distributed as shown in figure 15, with peaks at the connections of the wires. At these locations the electrodes' current density has a maximum, thereby also the power loss owns its maximum there, compare equation (23). In table 4, the numerically obtained values of the viscous power loss density p^{vis}, the polymers resistive power loss density p^{leak} and the maximum of the electrodes' resistive power loss density $\hat{p}^{\mathrm{res}}$ are given for the investigated frequencies. Comparing the sources of power losses by the proportion of the cumulated amount, one finds out, that the total viscous power loss P^{vis} is quite small and does not contribute significantly to the heating of the DEA. For frequencies up to $f = 190$ Hz, the leakage current in the polymer is the dominant cause for the total power loss. At higher frequencies, the electrodes' resistive power loss becomes the major contributor of the total power loss.

Table 2. Geometric dimensions and characteristics of the test-DEA.

Stack	Unit Cell Test Case 1	Unit Cell Test Case 2
number of active dielectric layers $n = 49$	$h_{\mathrm{d}} = 45\,\mu\mathrm{m}$ heat transfer constant lateral surface $h_{\mathrm{e}} = 5\,\mu\mathrm{m}$ $d = 5.8\,\mathrm{mm}$	$h_{\mathrm{d}} = 45\,\mu\mathrm{m}$ $h_{\mathrm{e}} = 5\,\mu\mathrm{m}$ $d_{\mathrm{a}} = 40\,\mathrm{mm}$ $d_{\mathrm{t}} = 50\,\mathrm{mm}$ $l = 22\,\mathrm{mm}$

Table 3. Material parameters of the numerical simulation.

Description	Symbol	Value
Mechanical material properties		
OGDEN-model stiffness	μ_1	$6.3 \times 10^5\ \mathrm{N\,m^{-2}}$
	μ_2	$1.2 \times 10^3\ \mathrm{N\,m^{-2}}$
	μ_3	$-1 \times 10^4\ \mathrm{N\,m^{-2}}$
OGDEN-model exponent	α_1	1.3
	α_2	5
	α_3	-2
PRONY-model decay factor	β_1	1.3×10^{-1}
	β_2	7.5×10^{-2}
	β_3	2.3×10^{-2}
PRONY-model decay time	τ_1	$2.2 \times 10^{-2}\ \mathrm{s}$
	τ_2	$4.0 \times 10^{-1}\ \mathrm{s}$
	τ_3	$3.2 \times 10^{1}\ \mathrm{s}$
mass density	ϱ	$1 \times 10^3\ \mathrm{kg\,m^{-3}}$
Electrodynamical material properties		
relative permittivity of polymer	ϵ_{r}	3
specific resistance of electrode	ρ_{e}	$5 \times 10^{-2}\ \Omega\mathrm{m}$
specific resistance of polymer	ρ_{d}	$1 \times 10^{-10}\ \Omega\mathrm{m}$
Thermodynamical material properties		
thermal conductivity of polymer	κ_{d}	$2 \times 10^{-1}\ \mathrm{W\,(Km)^{-1}}$
thermal conductivity of electrode	κ_{e}	$2.5\ \mathrm{W\,(Km)^{-1}}$
specific heat capacity of polymer	χ_{d}	$1.4 \times 10^3\ \mathrm{J\,(kgK)^{-1}}$
specific heat capacity of electrode	χ_{e}	$7 \times 10^2\ \mathrm{J\,(kgK)^{-1}}$
heat transfer constant top surface	β_T	$4.19\ \mathrm{W\,(K^{1.25}m^2)^{-1}}$
heat transfer constant lateral surface	α_L	$1.41\ \mathrm{W\,(Km^2)^{-1}}$
heat transfer constant lateral surface	β_L	$4.00\ \mathrm{W\,(K^{1.25}m^2)^{-1}}$

Nevertheless, the local heating of the structure is primarily defined by the local values of the power loss density p. For all investigated frequencies, the hot spots always occurred at the wires, which can be explained (i) by the superposition of all three regarded contributions for power loss and (ii) by the maximum of the electrodes" resistive power loss density p^{res} in this area.

5.3. Results of the simulation of the thermal field

In this section the results of the thermal field analysis are given. For this, the input load for the heat generation due to mechanical and electrical power losses were determined in section 5.2. In figure 16 the thermography of the DE test-structure is shown, gained by the numerical simulation with
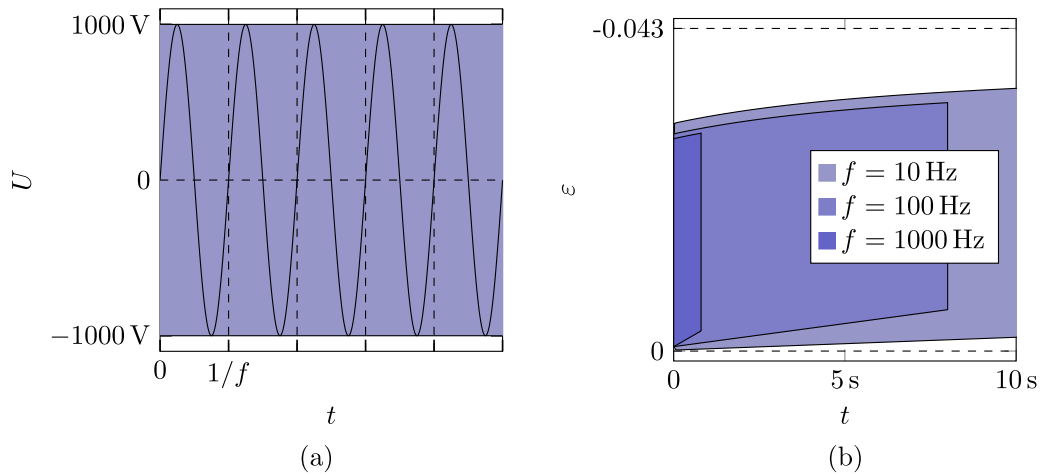
Figure 13. (a) Sinusoidal voltage excitation, filled background marks the amplitude of the oscillation and (b) the envelope of the response strain, the stationary state is established in a few seconds.
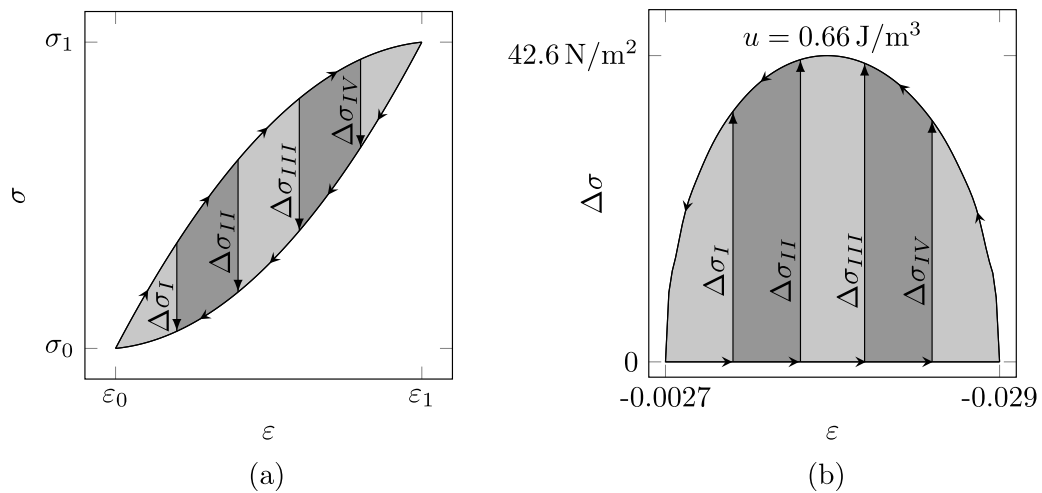

Figure 14. (a) Exemplary hysteresis plot, (b) Difference between the loading phase (lower graph) and unloading phase (upper graph) of the sinusoidal excitation of $U = 1\,\text{kV}$ and $f = 1\,\text{kHz}$.
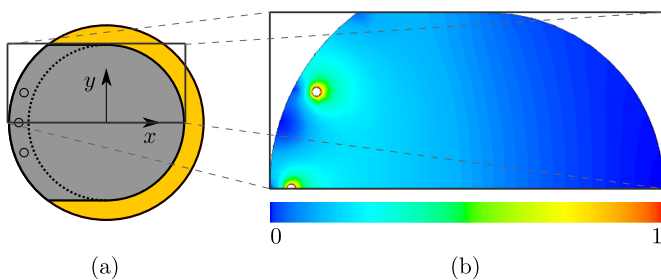

Figure 15. (a) section used for numerical investigation (half model), using symmetry conditions, (b) normalized distribution of the electric current $|\vec{i}|/|\vec{i}|_{\max}$ on the electrode layer.

a cyclic excitation of $U = 1\,\text{kV}$ and $f = 1\,\text{kHz}$. As expected, the highest temperatures occur at the connection wires. As can be seen, the whole structure heats up with increasing time. For locations at point No. 1 (in the middle) and point No. 2 (near the hot spots) the computed temperatures versus time

are shown figure 17. One may notice, that the temperatures are higher for higher frequencies.

6. Conclusion and outlook

In the present research, the thermal behavior of a dielectric elastomer test-structure under a cyclic electro-mechanical load was investigated, both experimentally and numerically.

In the experimental part, the thermo-electro-mechanical behavior of dielectric elastomer actuators has been investigated: for a cyclic actuation, the heating of the composite structure consisting of polymer and electrode layers has been studied. It has been shown, that the temperature increases with time and is maximal near the electrical connections. The obtained mechanical and electrical parameters are used for the numerical study.

In the modeling and simulation part, a one-way coupled thermo-electro-mechanical material model is presented. By

Table 4. Calculated power loss density for examined frequencies.

Frequency	p^{vis}	p^{leak}	$\hat{p}^{\text{res}}$
10 Hz	5.00×10^2 W m^{-3}	2.70×10^4 W m^{-3}	2.11×10^4 W m^{-3}
100 Hz	1.27×10^3 W m^{-3}	2.69×10^4 W m^{-3}	2.11×10^6 W m^{-3}
1000 Hz	1.32×10^3 W m^{-3}	2.69×10^4 W m^{-3}	2.12×10^6 W m^{-3}
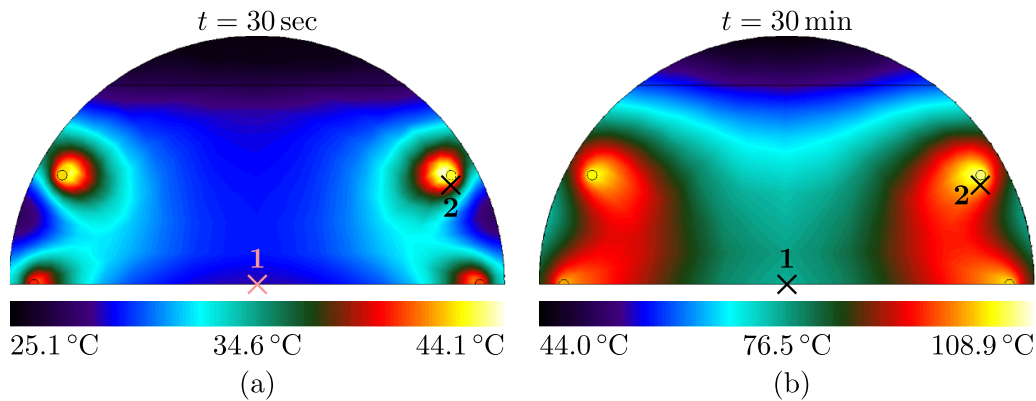
Figure 16. Plot of the numerically computed surface temperature of the sample DEA subjected to a dynamic excitation of 1 kV and 1 kHz, (a) after 30 seconds and (b) after 30 minutes. (Please consider the different temperature scales).
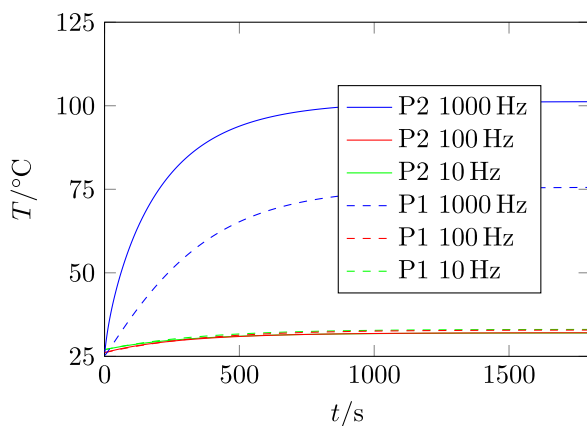
Figure 17. Heating of the test DEA due to the frequency of the applied voltage, at point No. 1 and point No. 2 (see figure 16), computed results.

using a linear electrical model and a visco-hyper-elastic mechanical model, the dissipation of the energy-transformation and thus the heat production was calculated, in order to obtain the input for the simulation of the thermal field. Concluding, this generated heat leads to a temperature increase of the DE test-structure, until a thermal equilibrium is reached. We have shown that the mechanical dissipation leads to a very low global heating in the active domain, whereas the electrical dissipation leads to a much higher heating, which is inhomogeneous in the electrodes'. This inhomogeneous heating reaches a maximum at the wires, as expected.

It has been shown that the experimentally and numerically obtained surface temperatures of the DEA match quite well. The maximal values in the experiment are a little bit higher than in the numerical simulation. This confirms that an application of temperature-dependent material parameters and the integration of thermal degradation phenomena are necessary. Also it is necessary to determine strain-dependent electrical parameters (e.g. resistivity and permittivity) as also mentioned by [39]. These aspects will be investigated in further research.

ORCID iDs

Florentine Förster-Zügel https://orcid.org/0000-0003-3111-146X
Thomas Wallmersperger https://orcid.org/0000-0002-4720-5260

References

[1] Förster F and Schlaak H F 2014 Optimized deformation behavior of a dielectric elastomer generator *Proc. SPIE* **9056** 905637
[2] Madden J, Vandesteeg N, Anquetil P, Madden P, Takshi A, Pytel R, Lafontaine S, Wieringa P and Hunter I 2004 Artificial muscle technology: physical principles and naval prospects *Oceanic Eng. J. IEEE* **29** 706–28
[3] Giousouf M and Kovacs G 2013 Dielectric elastomer actuators used for pneumatic valve technology *Smart Mater. Struct.* **22** 104010
[4] Baechler C, Gardin S, Abuhimd H and Kovacs G 2016 Inkjet printed multiwall carbon nanotube electrodes' for dielectric elastomer actuators *Smart Mater. Struct.* **25** 055009
[5] Carpi F *et al* 2015 Standards for dielectric elastomer transducers *Smart Mater. Struct.* **24** 105025
[6] Röntgen W C 1880 Ueber die durch Electricität bewirkten Form- und Volumenänderungen von dielectrischen Körpern *Ann. Phys., Lpz.* **247** 771–86
[7] Pelrine R E, Kornbluh R D and Joseph J P 1998 Electrostriction of polymer dielectrics with compliant

electrodes' as a means of actuation *Sensors Actuators* A **64** 77–85

[8] Kornbluh R D, Pelrine R, Pei Q, Oh S and Joseph J 2000 Ultrahigh strain response of field-actuated elastomeric polymers *Proc. SPIE* **3987** 51–64

[9] Benslimane M, Gravesen P and Sommer-Larsen P 2002 Mechanical properties of dielectric elastomer actuators with smart metallic compliant electrodes' *Proc. SPIE* **4695** 150–7

[10] Ask A, Menzel A and Ristinmaa M 2012 Phenomenological modeling of viscous electrostrictive polymers *Int. J. Non-Linear Mech.* **47** 156–65

[11] Büschel A, Klinkel S and Wagner W 2013 Dielectric elastomers – numerical modeling of nonlinear visco-electroelasticity *Int. J. Numer. Methods Eng.* **93** 834–56

[12] Mößinger H, Förster-Zügel F and Schlaak H F 2016 Simulation of the transient electromechanical behaviour of dielectric elastomer transducers *Proc. SPIE* **9798** 979831

[13] Madsen F B, Daugaard A E, Hvilsted S and Skov A L 2016 The current state of silicone-based dielectric elastomer transducers *Macromol. Rapid Commun.* **37** 378–413

[14] Schlögl T and Leyendecker S 2016 Electrostatic–viscoelastic finite element model of dielectric actuators *Comput. Methods Appl. Mech. Eng.* **299** 421–39

[15] Wissler M and Mazza E 2005 Modeling and simulation of dielectric elastomer actuators *Smart Mater. Struct.* **14** 1396–402

[16] Lucking Bigué J-P, Chouinard P, Denninger M, Proulx S and Plante J-S 2010 Thermodynamic model using experimental loss factors for dielectric elastomer actuator design *Proc. SPIE* **7642** 76420T

[17] Lotz P, Matysek M and Schlaak H F 2011 Lifetime of dielectric elastomer stack actuators *Proc. SPIE* **7976** 79760P

[18] Duduta M, Hajiesmaili E, Zhao H, Wood R J and Clarke D R 2019 Realizing the potential of dielectric elastomer artificial muscles *Proc. Natl Acad. Sci.* **116** 2476–81

[19] Christensen L R, Hassager O and Skov A L 2019 Electro-thermal model of thermal breakdown in multilayered dielectric elastomers *AIChE J.* **65** 859–64

[20] Kleo M, Mösinger H, Förster-Zügel F, Schlaak H F and Wallmersperger T 2018 Investigation of the thermal effects in dynamically driven dielectric elastomer actuators *Proc. SPIE* **10594** 105940G

[21] Zhao X, Koh S J A and Suo Z 2011 Nonequilibrium thermodynamics of dielectric elastomers *Int. J. Appl. Mech.* **03** 203–17

[22] Haus H, Matysek M, Mösinger H and Schlaak H F 2013 Modelling and characterization of dielectric elastomer stack actuators *Smart Mater. Struct.* **22** 104009

[23] Flittner K 2015 Dielektrische Elastomerstapelaktoren für Mikroventile *PhD Thesis* Technische Universität Darmstadt

[24] Matysek M 2010 Dielektrische Elastomeraktoren in Multilayer-Technologie für taktile Displays *PhD Thesis* Technische Universität Darmstadt

[25] Matysek M, Lotz P, Flittner K and Schlaak H F 2008 High-precision characterization of dielectric elastomer stack actuators and their material parameters *Proc. SPIE* **6927** 692722

[26] Ogden R W 1972 Large Deformation Isotropic Elasticity - On the Correlation of Theory and Experiment for Incompressible Rubberlike Solids *Proc. R. Soc.* A **326** 565–84

[27] Briody C, Duignan B, Jerrams S and Tiernan J 2012 The implementation of a visco-hyperelastic numerical material model for simulating the behaviour of polymer foam materials *Comput. Mater. Sci.* vol 64 pp 47–51 Proc. of the 21st Int. Workshop on Computational Mechanics of Materials (IWCMM 21)

[28] Henke E-F M, Wilson K E and Anderson I A 2018 Modeling of dielectric elastomer oscillators for soft biomimetic applications *Bioinspir. Biomim.* **13** 046009

[29] Tschoegl N W 1989 *The Phenomenological Theory of Linear Viscoelastic Behavior: An Introduction* (Berlin: Springer)

[30] Madsen F B, Yu L, Hvilsted S and Skov A L 2015 Super soft silicone elastomers with high dielectric permittivity *Proc. SPIE* **9430** 94301D

[31] Foo C C, Cai S, Koh S J A, Bauer S and Suo Z 2012 Model of dissipative dielectric elastomers *J. Appl. Phys.* **111** 034102

[32] Eringen A C 1990 *Electrodynamics of Continua - 1 : Foundations and Solid Media* (New York, Heidelberg: Springer)

[33] Incropera F P, DeWitt D P, Bergman T L and Lavine A S 2007 *Fundamentals of Heat and Mass Transfer* Hoboken N J ed 6 [ua] (New York: Wiley)

[34] Bai E-W and Lonngren K E 2004 Capacitors and the method of moments *Comput. Electr. Eng.* **30** 223–9

[35] Lochmatter P 2007 Development of a shell-like electroactive polymer (EAP) actuator *PhD Thesis* ETH Zurich

[36] Wacker Chemie A G (www.wacker.com/cms/en /products/product/product.jsp?product=12924) retrieved November 01, 2019

[37] Huang X, Jiang P and Tanaka T 2011 A review of dielectric polymer composites with high thermal conductivity *IEEE Electr. Insul. Mag.* **27** 8–16

[38] Zhou W, Wang C, An Q and Ou H 2008 Thermal properties of heat conductive silicone rubber filled with hybrid fillers *J. Compos. Mater.* **42** 173–87

[39] Zhao X and Suo Z 2008 Electrostriction in elastic dielectrics undergoing large deformation *J. Appl. Phys.* **104** 123530